ISSN: 0974-5823 Vol. 7 No. 5 May, 2022

*International Journal of Mechanical Engineering*

# Optical and Magnetic Properties of Chromium Doped $Pr_{0.5}Sr_{0.5}MnO_3$ System

**Ashok Kumar Kusuma[1,2], Katrapally Vijaya Kumar[1]*, A. T. Raghavender[3]**

[1]Department of Physics, JNTUH University College of Engineering Rajanna Sircilla, Agraharam, Rajanna Sircilla-District, 505302, TS, India.

[2]B V Raju Institute of Technology, Narsapur, 502 313, Telangana, India.

[3]Department of Physics, International School of Technology and Sciences for Women, Rajamahendravaram, East Godavari – 533 294, Andhra Pradesh, India.

*Corresponding author :Katrapally Vijaya Kumar

**Abstract**

Chromium doped $Pr_{0.5}Sr_{0.5}Mn_{1-x}Cr_xO_3$ (x= 0.0, 0.1, 0.2, 0.3, 0.4) samples were synthesized using sol-gel method. The structural, optical and magnetic properties were measured using XRD, XPS, UV-Vis Spectroscopy, Raman spectroscopy and room temperature VSM. It was observed from the XRD analysis that all the samples revealed the formation of single-phase structure without any secondary phases. The crystallite size was observed to increase with increasing Cr coping content. XPS analysis revealed the presence of the composition $Pr_{0.5}Sr_{0.5}Mn_{1-x}Cr_xO_3$ (x= 0.0, 0.1, 0.2, 0.3, 0.4) and dual oxidation states of $Mn^{3+}$ and $Mn^{4+}$. From UV-Vis spectra, energy bandgaps were calculated and found in the range 1.17 ev to 0.52 eV, which could be attributed due to the electronic transition from up-spin of $Mn^{3+}$ ion and down-spin of an adjacent $Mn^{4+}$ ion. The characteristic peaks in Raman spectra was observed in the frequency range 200-1000 $cm^{-1}$, at different measurement temperatures. The Raman spectra exhibited an additional high frequency mode attributed to the local vibration of oxygen surrounding substituent ion. It was observed that the frequency and intensity of Raman spectra were sensitive to the temperature and doping concentration. Magnetization data at room temperature for undoped sample showed magnetization curve and for doped samples they showed paramagnetic behavior.

*Keywords: CMR materials, XRD, XPS, UV-Vis spectroscopy, Raman spectroscopy, Magnetic Properties*

## 1.Introduction

Colossal Magneto Resistance (CMR) manganites are capable of exhibiting the coexistence of metallic conductivity along with ferromagnetic behavior at low temperatures (below *T*c) and insulating behavior along with paramagnetic behavior at high temperatures (above *T*c). The double exchange mechanism was used by Zener [1] to explain correlation between metallic conductivity and ferromagnetism in these materials. Further Millis et al. [2], suggested that the double exchange mechanism alone cannot account for the magnitude of the resistivity drop below *T*c and the electron–phonon coupling, originally due to Jahn Teller distortion, might also play an important role among CMR materials. Thus, this most interesting motivating and effective behavior exhibited of CMR materials fascinated research community in studying structural, magnetic and electrical transport properties and their potential applications in memory devices [3-5]. Among these CMR materials, the charge-ordered phase in half-doped manganites, with compositions, $R_{0.5}A_{0.5}MnO_3$ (R = La, Pr, Sm, and Nd; A = Sr and Ca) exhibits interesting phenomena such as charge, orbital, and spin ordering, along with magnetic and electric field driven transitions [6,7]. Moreover, it was reported that doping with Cr in the place of Mn site is an effective way to modify the charge ordered (CO)/orbital ordered (OO) and anti-ferromagnetic insulating (AFMI) phases. As the $Cr^{3+}$ ion is iso-electronic with $Mn^{4+}$ ion, Mn site substitutions with Cr in manganites have attracted great interest. Magnetic impurities such as Cr and Ru at the Mn site can effectively induce both metallicity and ferromagnetism in the insulating antiferromagnetic $R_{0.5}A_{0.5}MnO_3$ (A = Ca, Sr) [8, 9]. It was reported that among the dopants, chromium is the most efficient one to induce a metal insulator transition in charge ordered undoped insulators, and lead to a much higher CMR effect [10-12].

Finally, in the theory of solids, study of the elastic behavior has particular significance in understanding the nature of inter atomic and inter ionic forces in them [13]. Further, the general idea of elastic moduli values that characterize mechanical strength, fracture toughness and thermal shock resistance will be useful in study the high strains that might develop when ceramic perovskites are subjected to a high magnetic field [14]. Moreover, the ultrasonic velocity measuring technique is a non-destructive one and is a very sensitive tool not only for studying the defects of microscopic process in solids but also most conventional technique for determination of elastic constants [15]. In view of this, the influence of Cr ion doping on structural and elastic behavior of $Pr_{0.5}Sr_{0.5}Mn_{1-x}Cr_xO_3$(x= 0, 0.1, 0.2, 0.3 & 0.4) system is presented in this article.

## 2. Experiment

Polycrystalline $Pr_{0.5}Sr_{0.5}Mn_{1-x}Cr_xO_3$ (x=0, 0.1, 0.2, 0.3 & 0.4) samples were synthesized by the sol–gel method [16 - 18] using pure metal nitrates as the initial materials (99.9 % pure). The compositions of the samples are henceforth designated as PSMCO-0, PSMCO-1, PSMCO-2, PSMCO-3 and PSMCO-4 respectively. These powders were calcined at 1100°C for 8h followed by sintering at 1300°C for 4h in air. The structural characterization was carried out by powder X-ray diffraction (XRD) using Phillips

expert diffractometer at room temperature in the 2θ range of 20-80º. Fourier transform infrared spectroscopy (FTIR) was recorded on a Jasco FTIR spectrometer (Model: FT/IR-4200typeA) within a range of 400–4000 $cm^{-1}$. The Raman spectroscopy measurements were performed using Raman spectrometer (Lab RAM Horiba France) with two grating, using 532nm Nd-YAG laser 100 mW. XPS measurements for PSMCO-4 sample at room temperature were undertaken by XPS spectrometer. Magnetic measurements were performed using vibrating sample magnetometer (VSM) 7410S.

**3. Result and Discussion**

XRD patterns of all the samples $Pr_{0.5}Sr_{0.5}Mn_{1-x}Cr_xO_3$ (x= 0.0, 0.1, 0.2, 0.3, 0.4) as shown in the Fig.1 revealed the formation of single-phase structure without any impurities [9]. The Rietveld refinement technique [17, 18] confirmed the that all the synthesized samples belong to orthorhombic structure (Pnma space group). The crystallite size was observed to increase from 26.12 nm to 32.92 nm with the increase in Cr doping content. It was observed that, there is no significant variation in lattice parameters with doping concentrations. This kind of behavior in the lattice parameters may be attributed due to the fact that, there is little difference in the ionic radii between $Cr^{3+}$ and $Mn^{3+}$ ions [19].

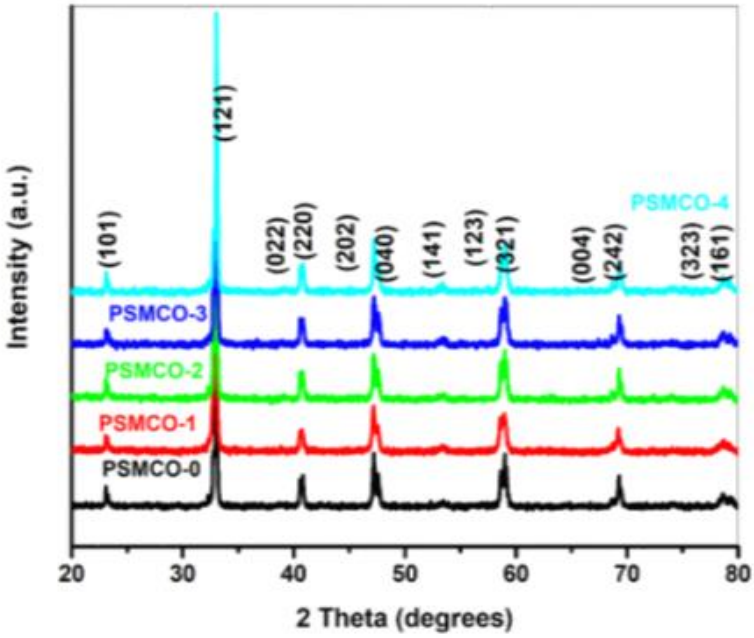


Figure 1. XRD pattern of $Pr_{0.5}Sr_{0.5}Mn_{1-x}$ $Cr_xO_3$ (x= 0.0, 0.1, 0.2, 0.3, 0.4) system.

**3.1 Raman scattering**

Raman spectroscopy is used to study the lattice distortion [20, 21] in PSMCO system. Fig.2 shows the Raman spectra of $Pr_{0.5}Sr_{0.5}Mn_{1-x}Cr_xO_3$ (x= 0.0, 0.1, 0.2, 0.3, 0.4) samples at different temperatures. At room temperature the Raman spectra is as shown in Fig. 2(a). From the Raman spectra, two peaks were observed at 862, 888 $cm^{-1}$ for PSMCO-0 sample, one peak was observed at 843 $cm^{-1}$ for PSMCO-1 sample, there no peaks observed for PSMCO-2, two peaks were observed for at 862, 888 $cm^{-1}$ for PSMCO-3 sample, whereas the six peaks were observed at 346, 370, 400, 862, 888, 909 $cm^{-1}$ for PSMCO-4 sample.

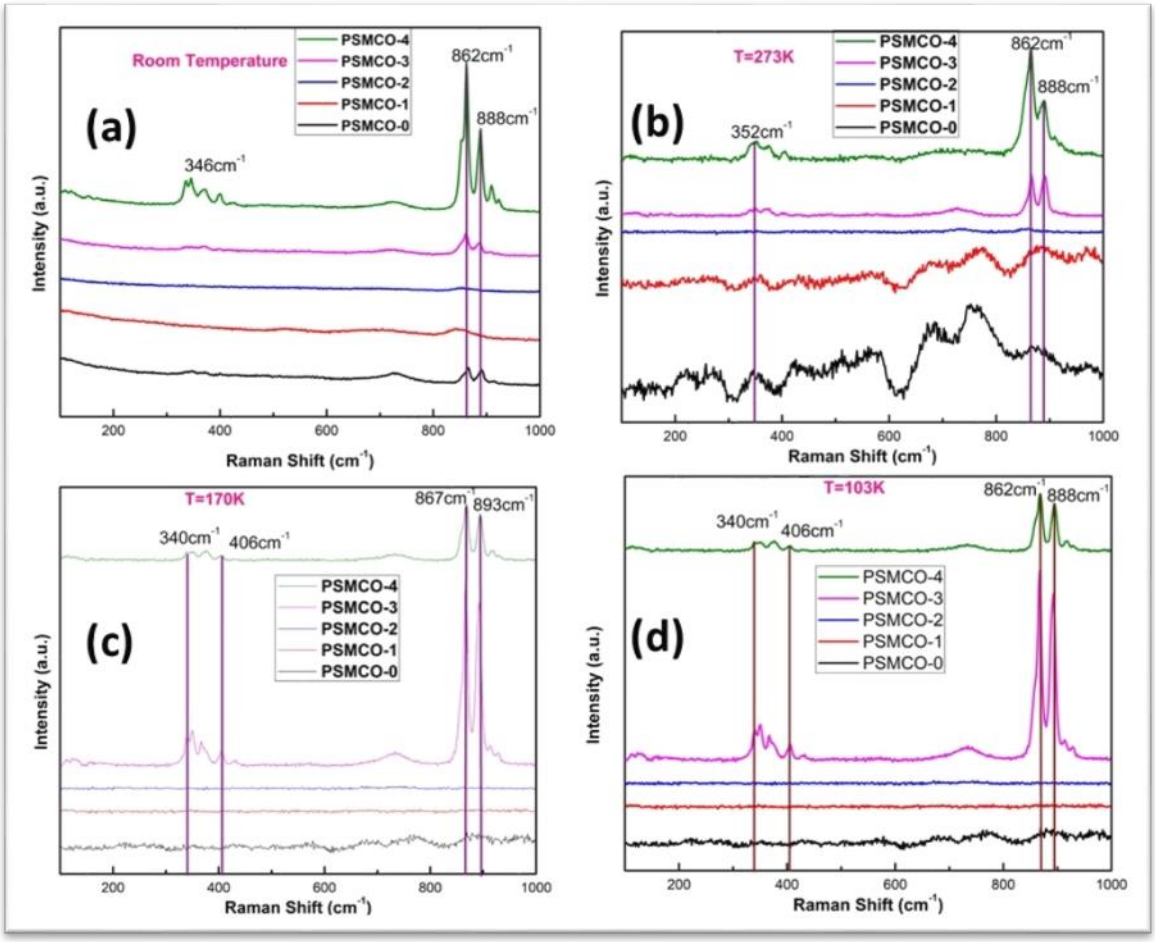


Figure 2. Raman spectra of $Pr_{0.5}Sr_{0.5}Mn_{1-x}$ $Cr_xO_3$ (x= 0.0, 0.1, 0.2, 0.3, 0.4) system at different temperatures.

It is observed that Cr doping has significant effect on the structural properties of $Pr_{0.5}Sr_{0.5}Mn_{1-x}$ $Cr_xO_3$, causing appearance of different characteristic peaks with different intensities and at different positions. The peak intensity at 862 $cm^{-1}$ associated with $MnO_6$ vibrations increased in intensity with increasing Cr doping content (x). This is caused by Cr doping-induced local strain in structure, which changes the atomic vibration frequencies [20 - 26]. Raman spectra of PSMCO system at 273K temperature is shown in Fig. 2(b), the Raman spectra shows that, there is no evidence of characteristic peaks for PSMCO-0, PSMCO-1 and PSMCO-2 samples. The peak position due to $MnO_6$ remained same for PSMCO-3 and PSMCO-4, apart from 862 $cm^{-1}$ peak few other peaks also appeared at 352, 368, 728, 888 $cm^{-1}$ for PSMCO-3 and 352, 373, 404, 888 $cm^{-1}$ for PSMCO-4 samples. Raman spectra of all PSMCO system recorded at 170K is shown in Fig. 2(c). Raman spectra revealed that the peaks do not appear for PSMCO-0, PSMCO-1 and PSMCO-2 samples. Whereas Raman appeared at 340, 350, 366, 406, 428, 734, 867, 893 $cm^{-1}$ for PSMCO-3 and 340, 373, 406, 867, 893, 917 $cm^{-1}$ for PSMCO-4 samples. At 170K, there was slight shift in the $MnO_6$ peak position. Raman spectra recorded at 103K is shown in Fig. 2(d). Raman spectra that the peaks do not appear for PSMCO-0, PSMCO-1 and PSMCO-2 samples. Raman appeared at 340, 350, 368, 406, 733, 862, 888, 914, 927 $cm^{-1}$ for PSMCO-3 and 340, 377, 406, 862, 888, 915 $cm^{-1}$ for PSMCO-4 samples. These Raman peaks observed at different temperatures are presented in Table 1. The appearance of specific peaks for each sample in Raman spectra reveals the characteristic behavior of synthesized samples.

**3.2 XPS spectra**

To estimate composition and ionic valance states in the synthesized samples, XPS measurements were conducted. The XPS spectrum for a typical sample PSMCO-4 is shown in Fig. 3. The XPS spectra shows the presence of all expected elements, Pr, Sr, Mn, Cr, O, C in the synthesized system [27-29].

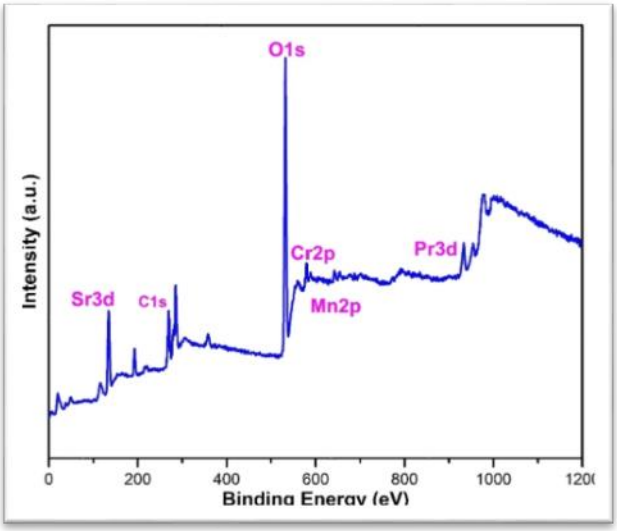


Figure 3. XPS spectra $Pr_{0.5}Sr_{0.5}Mn_{1-x}Cr_xO_3$ (x= 0.4) system.

Furthermore, the C1s peak present may be due to air contamination on the surface. The narrow scan of Pr 3d is shown in Fig.4(a) and its binding energy is 933.5eV. The narrow scan of Sr 3d is shown in Fig.4(b) and its binding energy is 134.27eV. The deconvoluted peaks of the $Mn2p_{3/2}$ and Mn $2p_{1/2}$ XPS peaks are shown in Fig. 4(c). XPS analysis clearly shows that, the Mn 2p XPS peak is deconvoluted into two peaks at 641.13 and 653.38 eV, corresponding to the $Mn^{3+}$ and $Mn^{4+}$ ions respectively. Narrow scan and fitting for Cr 2p is shown in Fig. 4(d). Two XPS peaks are located at 579.49 and 588.87 eV, which are assigned as Cr $2p_{3/2}$ and Cr $2p_{1/2}$, respectively due to the spin-orbit splitting. That indicates that Cr exists in +2 oxidation state. The Mn $2p_{3/2}$ and Mn $2p_{1/2}$ core levels are split into two peaks due to two valences of manganese upon $Cr^{2+}$ doping, which forms the root cause of the double exchange (DE) interaction. In addition, the content ratio of the $Mn^{3+}$ and $Mn^{4+}$ ions estimated from the deconvoluted XPS peak areas was approximately 2:1. Moreover the C1s XPS peak as shown in Fig.4(e) is observed at binding energy 284.84eV ( as adhesive carbon tape is used to attach in finding composition of samples). The narrow scan for O1s peak is shown in Fig. 3(f), is attributed due to the crystal lattice oxygen located at 531.98 eV.

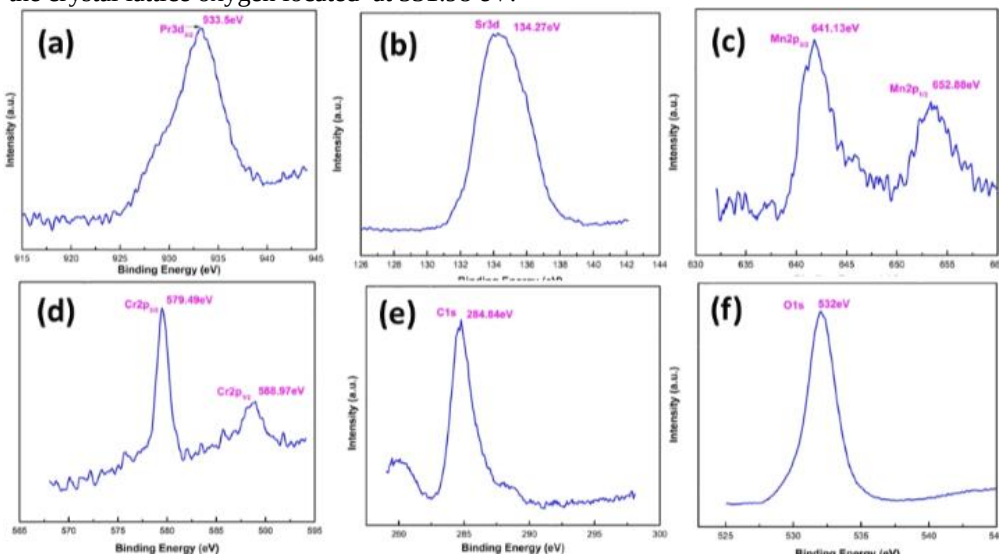


Figure 4. XPS spectra $Pr_{0.5}Sr_{0.5}Mn_{1-x}Cr_xO_3$ (x= 0.4) system narrow scan for Pr, Sr, Mn, Cr, C and O.

### 3.3 Optical Properties

Optical bandgaps of the $Pr_{0.5}Sr_{0.5}Mn_{1-x}Cr_xO_3$ (x= 0.0, 0.1, 0.2, 0.3, 0.4) samples were determined from UV-Vis absorption spectra and corresponding Tauc's plots are plotted as shown in Fig.5 for PSMCO-0, where hυ is incident light energy and absorption cofficient is denoted by α. The optical bandgap plots for PSMCO-1, PSMCO-2, PSMCO-3 and PSMCO-4 is shown in Fig's. 5 (a) – (e).

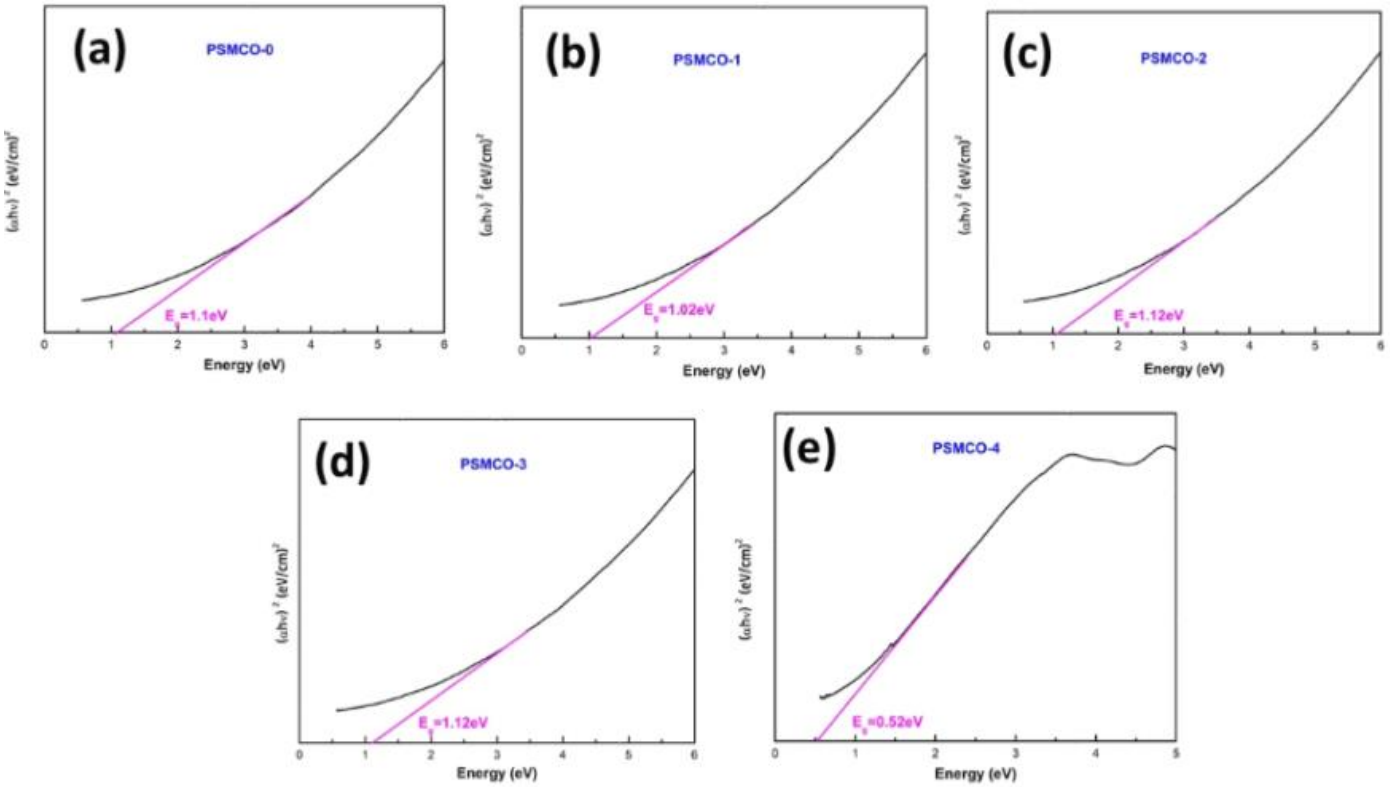


Figure 5. Tauc's plot for $Pr_{0.5}Sr_{0.5}Mn_{1-x}$ $Cr_xO_3$ (x= 0.0, 0.1, 0.2, 0.3, 0.4) system, (a) x = 0.0, (b) x = 0.1, (c) x = 0.2, (d) x = 0.3 and (e) x = 0.4.

The absorption coefficient of the ferrite nanoparticles has been determined from the absorption data by using the fundamental relationships (1, 2 and3) [30, 31].

$$I = I_0 e^{\alpha t} \quad \text{---(1)}$$

$$A = log \frac{I_0}{I} \quad \text{---(2)}$$

and $$\alpha = \frac{2.303(A)}{t} \quad \text{---(3)}$$

Where, α is absorption coefficient, A is the absorbance, and t is the thickness of the samples. To calculate the optical absorption for the present ferrite nanoparticles, the following Tauc's relation (4) [30, 31] is used

$$(\alpha h\nu)^{1/n} = A(h\nu - E_g) \quad \text{---(4)}$$

Where, α is absorption coefficient, h is plank's constant, ν is frequency, A is absorbance and $E_g$ is optical energy bandgap. $(\alpha h\nu)^{1/n}$ was plotted as a function of the photon energy (hν) for different n values (n=1/2, 3/2, 2, 3). For direct allowed transition n=1/2, indirect allowed transition n=2, direct forbidden transition n=3/2 and forbidden indirect transition n=3. To determine the possible transitions, $(\alpha h\nu)^2$ vs hν is plotted and corresponding optical energy bandgap were obtained from extrapolating the straight portion of the graph on hν axis.

The calculated optical bandgaps were observed in the range 1.17 – 0.52 eV, which are summaried in Table. 1. This optical bandgap range behaves similar to semiconductors ($E_g$ is in the range 0.5–2.5eV). In these samples Mn cations exist a mixed valence of $Mn^{3+}$ and $Mn^{4+}$, which are sorrounded by six $O^{2-}$ anions, forming $MnO_6$ octahedral structure. The optical bandgaps can be attributed to the electronic transition from up-spin of $Mn^{3+}$ ion and down-spin band of a adjacent $Mn^{4+}$ ion, and the energy difference between two bands is Hund's coupling energy.

Table 1. Energy band gaps and Raman peaks at different temperatures (Room Temp, 273K, 170K, 103K) for $Pr_{0.5}Sr_{0.5}Mn_{1-x}$ $Cr_xO_3$ (x= 0.0, 0.1, 0.2, 0.3, 0.4) system.

| **Sample code** | **Energy Gap (eV)** | **Raman Peaks ($cm^{-1}$) at different temperatures** | | | |
|---|---|---|---|---|---|
| | | **Room Temp** | **T=273K** | **T=170K** | **T=103K** |
| **PSMCO-0** | 1.17 | 862, 888 | --- | --- | --- |
| **PSMCO-1** | 1.02 | 843 | --- | --- | --- |
| **PSMCO-2** | 1.12 | --- | --- | --- | --- |
| **PSMCO-3** | 1.12 | 862, 888 | 352, 368, 728, 862, 888 | 340, 350, 366, 406, 428, 734, 867, 893, | 340, 350, 368 406, 733, 862, 888, 914, 927 |
| **PSMCO-4** | 0.52 | 346, 370, 400, 862, 888, 909 | 352, 373, 404, 862, 888 | 340, 373, 406, 867, 893, 917 | 340, 377, 406, 862, 888, 915 |

### 3.5 Magnetic Properties

The magnetization measurments at room temperature was measured for $Pr_{0.5}Sr_{0.5}Mn_{1-x}Cr_xO_3$ (x= 0.0, 0.1, 0.2, 0.3, 0.4) samples and the obtained magnetization curves are plotted as shown in Fig. 6.

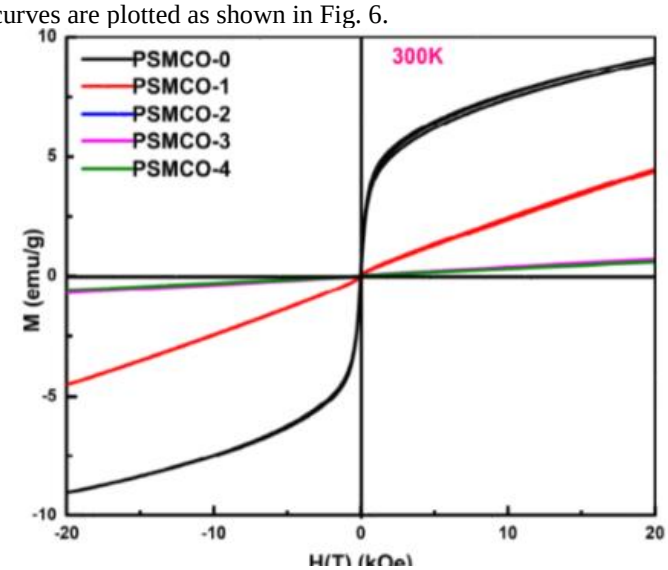


Figure 6. M-H plots for $Pr_{0.5}Sr_{0.5}Mn_{1-x}$ $Cr_xO_3$ (x= 0.0, 0.1, 0.2, 0.3, 0.4) system at 300K.

The undoped sample with Cr, x = 0.0 showed a narrow magnetization curve. The Cr content with x = 0.1 showed a linear curuve without any magnetization loops. For other samples with Cr, x = 0.2, 0.3 and 0.4 showed negligible magnetization. For sample with Cr, x = 0.1 to 0.4, the samples showed the paramagnetic behaviour at room temperature [32]. We did not see any significant effect of magnetization even with increasing chromium doping concentration in the samples. Infact the magnetization is suppressed with the increase in Cr doping in the samples.

### 4. Conclusions

In the present work chromium doped $Pr_{0.5}Sr_{0.5}Mn_{1-x}Cr_xO_3$ system (x= 0.0, 0.1, 0.2, 0.3, 0.4) manganites were prepared by sol-gel method. XRD patterns and Rietveld refinements demonstrated that all the synthesized samples were having orthorhombic structure with space group of Pnma. XPS analysis confirmed that Mn ions existed in dual chemical states of $Mn^{3+}$ and $Mn^{4+}$ with 2:1 ratio, Cr element was in stable divalent state and Nd element in trivalent state. The optical bandgaps calculated from UV- Vis absorption spectra were observed in the range 1.17 eV to 0.52 eV. The M-H plots recorded at room temperature for undoped samples showed ferromagnetic properties and for rest of the sample they showed the paramagnetic properties.

### References


[1] Zener, C. (1951) Interaction between the d-Shells in the Transition Metals. II. Ferromagnetic Compounds of Manganese with Perovskite Structure. Physical Review Journals Archive, 82, 403-405.

[2] Millis, A.J., Shraiman, B.I. and Mueller, R. (1996) Dynamic Jahn-Teller Effect and Colossal Magnetoresistance in $La_{1-x}Sr_xMnO_3$. Physical Review Letters, 77, 175-178.

[3] Dagotto, E., Hotta, T. and Moreo, A. (2001) Colossal Magnetoresistant Materials: The Key Role Of Phase Separation. Physics Reports, 344, 1-3.

[4] Tokura, Y. (2006) Critical Features of Colossal Magnetoresistive Manganites. Reports on Progress in Physics, 69, 797- 851.

[5] Hatano, T. (2013) Gate Control Of Electronic Phases in A Quarter-Filled Manganite. Scientific Reports, 3, 2904.

[6] Jin, S., Tiefel, H., Mc Cornack, M., Fastnacht, R.A., Ramesh, R. and Chen, L.H. (1994) Thousand fold Change in Resistivity in Magnetoresistive La-Ca-Mn-O Films. Science, 264, 413-415.

[7] Autret, C., Maignan, A., Martin,C., Hervieu, M., Hardy, V., He´bert, S. and Raveau, B. (2003) Magnetization Steps in A Noncharge-Ordered Manganite, $Pr_{0.5}Ba_{0.5}MnO_3$. Applied Physics Letters. 82, 4746-4748.

[8] Raveau, B., Maignan, A. and Martin, C. (1997) Insulator–Metal Transition Induced by Cr and Co Doping in $Pr_{0.5}Ca_{0.5}MnO_3$. Journal of Solid State Chemistry, 130, 162-166.

[9] Kimura, T., Tomioka, Y., Okimoto, Y. and Tokura, Y. (1999) Diffuse Phase Transition and Phase Separation in Cr-Doped $Nd_{1/2}Ca_{1/2}MnO_3$: A Relaxor Ferromagnet. Physical Review Letters, 83, 3940-3943.

[10] Barnabe, A., Maignan, A., Hervieu, M., Damay, F., Martin, C. and Raveau, B. (1997) Extension Of Colossal Magnetoresistance Properties to Small A Site Cations By Chromium Doping in $Ln_{0.5}Ca_{0.5}MnO_3$ Manganites. Applied Physics Letters, 71, 3907- 3909.

[11] Kimura, T., Kumai, R., Okimoto, Y., Tomioka, Y. and Tokura, Y. (2000) Variation of Charge-Orbital Correlation with Cr Doping in Manganites. Physical Review B,62, 15021- 15025.

[12] Young Sun, Wei Tong, Xiaojun Xu and Yuheng Zhang, (2001) Tuning Colossal Magnetoresistance Response by Cr Substitution In $La_{0.67}Sr_{0.33}MnO_3$. Applied Physics Letters, 78, 643-645.

[13] Lalitha, G., Das, D., Bahadur, D. and Venugopal Reddy, P. (2008) Elastic behavior of $La_{0.67}Ca_{0.33}MnO_3$:$ZrO_2$ composites. Journal of Alloys and Compounds, 464, 6-8.

[14] Buch, J.J.U., Lalitha, G., Pathak, T.K., Vasoya, N.H., Lakhani, V.K., Reddy, P.V., Ravi Kumar and Modi, K.B. (2008) Structural and elastic properties of Ca-substituted $LaMnO_3$ at 300K. Journal of Physics D: Applied Physics**,** 41**,** 025406(10pp).
[15] Wollan, E.O. and Koehler, W.C. (1955) Neutron Diffraction Study of the Magnetic Properties of the Series of Perovskite-Type Compounds [(1−x)La, xCa]$MnO_3$. Physical Review Journals Archive, 100, 545-563.
[16] A.T. Raghavender, D. Pajic, K. Zadro, T. Milekovic, P. V. Rao, K.M. Jadhav, D. Ravinder, J.Magn. Magn. Mater, 316 (2007) 1-7.
[17] Ashok Kumar Kusuma, Elle Sagar, Gundeti Sreeram Reddy, Katrapally Vijaya Kumar Bulgarian Journal of Physics vol. 48 (2021) 257–267.
[18] Ashok Kumar Kusuma, Elle Sagar, G Sreeram Reddy, and K. Vijaya Kumar, Adv. Nano. 10 (2021) 26-35.
[19] L. Ca Posna, A. Martinelli, M. G. Francesconi, P.G. Radaelli, R. Carvajal, O. Cebeza, M. Ferretti, C. Corridoni, N. Pompeo, Phys. Rev. B. 77 (2008) 104438.
[20] M.N. Iliev, M.V. Abrashev, H.-G. Lee, V.N. Popov, Y.Y. Sun, C. Thomsen, R.L. Meng, C.W. Chu, Raman spectroscopy of orthorhombic perovskite like YMnO3 and LaMnO3, Phys. Rev. B 57 (1998) 2872–2877.
[21] R. Krüger, B. Schulz, S. Naler, R. Rauer, D. Budelmann, J. Bäckström, K.H. Kim, S.- W. Cheong, V. Perebeinos, M. Rübhausen, Orbital ordering in LaMnO3 investigated by resonance Raman spectroscopy, Phys. Rev. Lett. 92 (2004) 097203.
[22] L. Martín-Carrón, A. de Andrés, Raman phonons and the Jahn–Teller transition in RMnO manganites, J. Alloy. Comp. 323–324 (2001) 417–421.
[23] M.N. Iliev, M.V. Abrashev, Raman phonons and Raman Jahn–Teller bands in perovskite-like manganites, J. Raman Spectrosc. 32 (2001) 805–811.
[24] M.V. Abrashev, A.P. Litvinchuk, M.N. Iliev, R.L. Meng, V.N. Popov, V.G. Ivanov, R.A. Chakalov, C. Thomsen, Comparative study of optical phonons in the rhombohedrally distorted perovskites LaAlO3 and LaMnO3, Phys. Rev. B 59 (1999) 4146–4153.
[25] M.A. Quijada, J.R. Simpson, L. Vasiliu-Doloc, J.W. Lynn, H.D. Drew, Y.M. Mukovskii, S.G. Karabashev, Temperature dependence of low-lying electronic excitations of LaMnO3, Phys. Rev. B 64 (2001) 224426.
[26] A.S. Moskvin, A.A. Makhnev, L.V. Nomerovannaya, N.N. Loshkareva, A.M. Balbashov, Interplay of p-d and d-d charge transfer transitions in rare-earth perovskite manganites, Phys. Rev. B 82 (2010) 035106
[27] R. Dudric, A. Vladescu, V. Rednic, M. Neumann, I. G. Deac, and R. Tetean, J. Mol. Struct. 1073, 66(2014).
[28] D. J. Lam, B. W. Veal, and D. E. Ellis, Phys. Rev. B 22, 5730 (1980).
[29] A. P. Grosvenor, R. G. Cavell, and A. Mar, Chem. Mater. 18, 1650 (2006).
[30] J. Tauc, R. Grigorovici, and A. Vancu, "Optical properties and electronic structure of amorphous germanium," Phys. Status Solidi 15, 627–637 (1966).
[31] A.T. Raghavender, A.P. Samantilleke, Pedro Sa, B.G. Almeida, M.I. Vasilevskiy, Nguyen Hoa Hong. Mater. Lett. 69 (2012) 59 – 62.
[32] J. S. Arafat, Ceramica, 66 (2020) 114 – 118.